A Multi-frame Image Speckle Denoising Method Based on Compressed Sensing Using Tensor Model

Ruofei Zhou, Gang Wang(✉), Wenchao Yang, Zhen Li, and Yao Xu

Harbin Institute of Technology, Harbin, China
zhouruofei0303@126.com, lizhen530l@126.com,
{gwang5l,wenchaoy}@hit.edu.cn

Abstract. Due to the bad channel environment and poor image sampling equipment, images are often contaminated by noise in the process of collection, transmission and processing. Speckle noise, which is difficult and complex to eliminate, is one of the common noise appearing in image processing. Denoising methods based on Compressed Sensing (CS) technology have been proved as useful tools in suppressing speckle noise of single-frame images. However, temporal correlation in multi-frame images has not yet been utilized. Considering that the traditional denoising methods do not work satisfactorily in speckle noise reduction, a multi-frame image speckle denoising methods based on compressed sensing using tensor model is proposed. The first step is to use the third-order tensor to represent the blocks of image sequences, then the denoising tensor model is established according to the CS theory and the corresponding optimization problem is raised. The problem is divided into three parts: the sparse representation, the tensor dictionary update and the image reconstruction. A Kruskal tensor-based Orthogonal Matching Pursuit (OMP) and Candecomp/Parafac (CP) analysis are used to solve these problems and get the denoised image. At last, simulations are conducted to compare the CS method and traditional methods. It is shown that the CS-based multi-frame speckle denoising method performs well in noise variance and can significantly enhance the visual quality of the image.

Keywords: Compressing sensing · Multi-frame image · Image denoising
Tensor factorization

1 Introduction

In the course of the collecting and processing of images, it is inevitable that image signal is polluted by noise. As a result, image denoising has always been a research focus in the field of image processing. For ultrasound images and radar images, which are formed from the reflection of the sound wave and electromagnetic wave, shade and light image particles would be produced when two echoes reflected by the target are overlapped. That is how speckle noise comes out in images, on account of the echo interference and disturbance between dispersive wave beams.

In recent years, certain amounts of speckle denoising methods have been proposed, in which filter denoising is the most widely used. For example, Lee filter [1] and Kuan

X. Gu et al. (Eds.): MLICOM 2017, Part II, LNICST 227, pp. 622–633, 2018.
https://doi.org/10.1007/978-3-319-73447-7_67

filter [2]. However, the size of filter window is difficult to choose. Although denoising effect turns out well, large size windows would lose most high frequency information. Small size windows fail in the ability of denoising, in spite of protecting detail information preferably. Aiming at solving this contradiction, several anisotropic diffusion have been presented, such as Perona-Malik Anisotropic Diffusion [3] (PMAD), Nonlinear Complex Diffusion Filter [4] (NCDF) and Speckle Reducing Anisotropic Diffusion [5] (SRAD). Nevertheless, these methods are likely to mix up image edges and speckle noises during edge detection.

A number of new speckle denoising methods have been suggested lately, for instance, Nonlinear Multi-scale Wavelet Diffusion [6] (NMWD) and Speckle Reduction Bilateral Filter [7] (SRBF). Compressed Sensing-based speckle denoising methods also perform well in speckle noise reduction of single-frame images. However, temporal correlation in multi-frame images has not yet been utilized.

In this paper, we focus on multi-frame image speckle denoising method based on Compressed Sensing using tensor model. Firstly, the third-order tensor is used to represent the blocks of image sequences. Not only is the information in spatial dimension kept, but also the information in temporal dimension is discovered. In the process of training the tensor sparse dictionary, temporal redundancy in video signals is utilized effectively. After the trained tensor sparse dictionary presents the images, output results will contain more information that is useful and noises will be separated extremely. The simulation results show that CS-based multi-frame speckle denoising method outperform traditional ways in terms of image quality and noise variance under the same conditions.

2 Speckle Denoising Tensor Model

2.1 Preliminaries

A tensor is also known as a multidimensional array, a higher dimensional form of data. A first-order tensor, as we know, is a vector. Moreover, a second-order tensor is a matrix. In addition, tensors of order three or higher are called higher-order tensors [8]. Multi-frame image cube is a typical third-order tensor. To distinguish higher order tensors from matrices, Higher-order tensors (order three or higher) are denoted by black letters. The nth order tensor is denoted by $\mathcal{A} \in \mathbb{R}^{I_1 \times I_2 \times \cdots I_N}$, and the number of all elements of $\mathcal{A}$ is $\prod_{j=1}^{N} I_j$. A third-order tensor is as shown in Fig. 1.

The outer product of two vectors U and V is:

$$U \otimes V = A = \begin{bmatrix} u_1 v_1 & u_1 v_2 & \cdots & u_1 v_n \\ u_2 v_1 & u_2 v_2 & \cdots & u_2 v_n \\ \vdots & \vdots & \ddots & \vdots \\ u_m v_1 & u_m v_2 & \cdots & u_m v_n \end{bmatrix} \tag{1}$$

where $U = (u_1, u_2, \cdots, u_m)$ and $V = (v_1, v_2, \cdots, v_n)$.

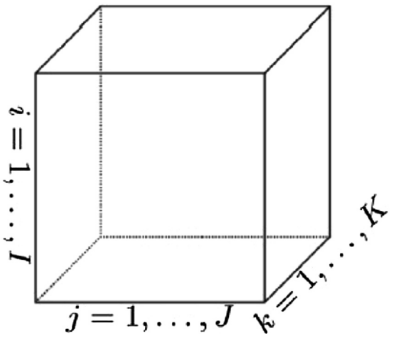

Fig. 1. A third-order tensor $\mathcal{A} \in \mathbb{R}^{I \times J \times K}$

And the Kronecker product of tensors $\mathcal{A}$ and $\mathcal{B}$ is defined by:

$$\mathcal{A} \otimes \mathcal{B} = \begin{bmatrix} a_{11}\mathcal{B} & a_{12}\mathcal{B} & \cdots & a_{1K}\mathcal{B} \\ a_{21}\mathcal{B} & a_{22}\mathcal{B} & \cdots & a_{2K}\mathcal{B} \\ \vdots & \vdots & \ddots & \vdots \\ a_{J1}\mathcal{B} & a_{J2}\mathcal{B} & \cdots & a_{JK}\mathcal{B} \end{bmatrix} \tag{2}$$

where $\mathcal{A} \in \mathbb{R}^{J \times K}$ and $\mathcal{B} \in \mathbb{R}^{M \times N}$.

After calculating the outer product, the number of dimensions of new tensor is the sum of two original tensors. For instance, $A \in R^{I_1 \times I_2 \times \cdots I_N}$ and $B \in R^{J_1 \times J_2 \times \cdots J_M}$, then $A \otimes B \in R^{I_1 \times I_2 \times \cdots I_N \times J_1 \times J_2 \times \cdots J_M}$. If N one-dimensional vector $K_i (i = 1, 2, \ldots, N)$, and the elements of each vector are $I_1, I_1, \ldots, I_N$, a N-order tensor $\mathcal{A}$ can be made up of these N one-dimensional vector $K_1 \circ K_2 \circ \cdots \circ K_N = \mathcal{A}$. The symbol "$\circ$" represents the vector outer product. An N-way tensor is rank one if it can be written as the outer product of N vectors. The process, in turn, of factorizing a tensor into a sum of component rank-one tensors is called the rank-one decomposition of $\mathcal{A}$. Proportional coefficients are needed sometimes, and then rank-one decomposition is defined by:

$$\mathcal{A} = CK_1 \circ K_2 \circ \cdots \circ K_N \tag{3}$$

However, most tensors are not rank-one. The rank of a tensor $\mathcal{A}$, denoted rank ($\mathcal{A}$), is defined as the smallest number of rank-one tensors that generate $\mathcal{A}$ as their sum. For formula (4), rank ($\mathcal{A}$) equals to the minimum R.

$$\mathcal{A} = \sum_{i=1}^{R} C_i K_{i1} \circ K_{i2} \circ \cdots \circ K_{iN} \tag{4}$$

2.2 Tensor Decomposition and Tensor Recovery

In the course of image processing, image recovery is necessary because images are often polluted by noises for some reason, even some parts of images are lost on the

receiving end. Using the characteristic low rank of images, images can be recovered by applying the low-rank recovery of matrices. In this way, the low-rank recovery method is applicable to recover any data that coincide the tensor model.

Kruskal decomposition and Tucker decomposition are two primary modes of tensor decomposition [9]. At first, Kruskal decomposition of a third-order tensor is introduced [10]. Consider a third-order tensor $\mathcal{X}$ of which the rank is R, i.e.,

$$\mathcal{X} = \sum_{i=1}^{R} \lambda_i \cdot a_i \circ b_i \circ \cdots \circ c_i \tag{5}$$

where A, B, C are rank-one component tensors of three directions, expressed as:

$$\begin{aligned} A &= [a_1, a_2, \ldots, a_R] \\ B &= [b_1, b_2, \ldots, b_R] \\ C &= [c_1, c_2, \ldots, c_R] \end{aligned} \tag{6}$$

So the Kruskal decomposition of $\mathcal{X}$ is illustrated in Fig. 2.

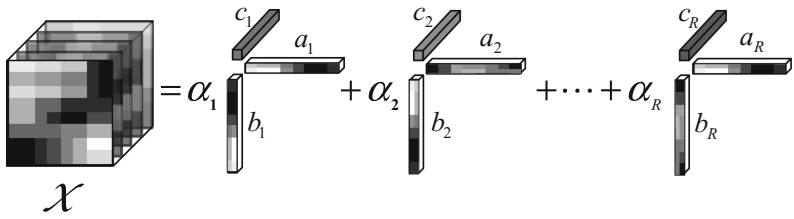

Fig. 2. Kruskal decomposition of a third-order tensor

The Tucker decomposition was first introduced by Tucker in [11] and refined in subsequent articles by Levin and Tucker. Let $\mathcal{X} \in \mathbb{R}^{X \times Y \times Z}$ be a three-way tensor and can be described as:

$$\begin{aligned} \mathcal{X} &= g \times_1 U \times_2 V \times_3 W \\ &= \sum_{r=1}^{R} \sum_{s=1}^{S} \sum_{t=1}^{T} g_{rst} u_r \circ v_s \circ w_t \end{aligned} \tag{7}$$

where $g \in \mathbb{R}^{R \times S \times T}$ is core tensor and $U \in \mathbb{R}^{X \times R}$, $V \in \mathbb{R}^{Y \times S}$, $W \in \mathbb{R}^{Z \times T}$ are three projection matrices of each direction.

The Tucker decomposition is a form of higher-order principal component analysis. It decomposes a tensor into a core tensor multiplied (or transformed) by a matrix along each mode. In some cases, the storage for the decomposed version of the tensor can be significantly smaller than for the original tensor. In the process of tensor recovery, original tensors can be generally recovered by arranging the coefficients of these components by values and adding the principal components.

So the Tucker decomposition of $\mathcal{X}$ is illustrated in Fig. 3.

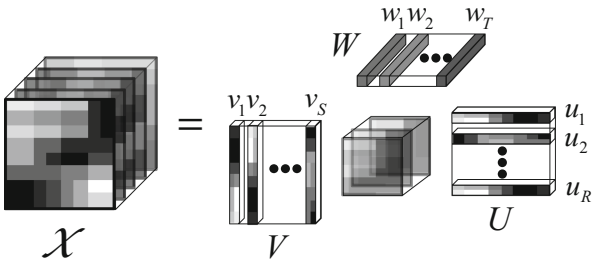

Fig. 3. Tucker decomposition of a third-order tensor

2.3 Multi-frame Image Denoising Tensor Model Based on CS

Because of the high sampling frequency in temporal dimension, contiguous frames are very similar in video data. As a result, there's a large amount of redundant information over each frame. In this paper, cardiac ultrasound video is used as research data. Cardiac ultrasound image sequences are shown in Fig. 4.

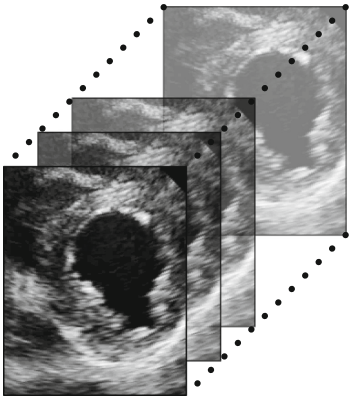

Fig. 4. Cardiac ultrasound image sequences

To begin with, images are divided into image blocks. After the sparse representation of these blocks, the integral image will be processed. The third-order Kruskal tensor model is introduced in the sparse representation of image block sequences, and the original images will be reconstructed by training the tensor dictionary. In this way, the loss of spatial information is avoided in the process of turning image blocks into one-dimensional signals. Meanwhile, the motional information of image blocks will be utilized for denoising by considering temporal information. The model can be generalized as:

$$\begin{aligned}\left\{\hat{\mathcal{X}}_k, \hat{\mathcal{D}}, \hat{A}\right\} = \arg\min_{\mathcal{D},\alpha_{ijt},\mathcal{X}} \lambda \left\| \frac{\mathcal{Y}-\mathcal{X}}{\sqrt{\mathcal{X}}} \right\|_F^2 \\ + \sum_{ij\in\Omega} \sum_{t=k-f+1}^{k+f-1} \mu_{ijt} \left\|\alpha_{ijt}\right\|_0 + \sum_{ij\in\Omega} \sum_{t=k-f+1}^{k+f-1} \left\|\mathcal{D}\alpha_{ijt} - R_{ijt}\mathcal{X}\right\|_F^2\end{aligned} \tag{8}$$

A third-order tensor representing noiseless image sequences is denoted by $\mathcal{X}$ The kth frame in $\mathcal{X}$ is denoted by $\mathcal{X}_k$, i.e. the noiseless form of the processing image. An image sequence that contains noise is denoted by $\mathcal{Y}$. An element of sparse coefficient matrix $A \in \mathbb{R}^{K\times N}$ is denoted by α_{ijt}, K is the number of atoms in dictionary and N equals to the number of blocks extracted from image sequences. The over-complete tensor dictionary is denoted by four-way tensor $\mathcal{D} \in \mathbb{R}^{m\times n\times f\times K}$, the estimation of kth noiseless frame is denoted by $\hat{\mathcal{X}}_k$, i.e. the resulting images after the process. When the optimal solution of this optimization problem is obtained, the over-complete tensor dictionary is denoted by $\hat{\mathcal{D}}$ and sparse coefficient matrix is denoted by $\hat{A}$. The position of blocks in integral image is denoted by μ_{ijt} and R_{ijt}, in which the elements are either 0 or 1.

To solve the optimization problem described by (8), we suggest two steps to get the results. Firstly, process the image block sequences and train the adaptive dictionary $\mathcal{D}$. Assuming that atoms of the tensor dictionary can represent each noiseless image sequence sparsely, we have $R_{ijt}\mathcal{X} = \mathcal{D}\alpha_{ijt}$. Then the optimization problem can be described as:

$$\left(\left\{\alpha_{ijt}\right\}^N, \mathcal{D}\right) = \arg\min_{\alpha_{ijt},\mathcal{D}} \sum_{ij\in\Omega} \sum_{t=1}^{T} \left(\mu_{ijt}\left\|\alpha_{ijt}\right\|_0 + \left\| \frac{R_{ijt}\mathcal{Y} - \mathcal{D}\alpha_{ijt}}{\sqrt{\mathcal{D}\alpha_{ijt}}} \right\|_F^2 \right) \tag{9}$$

It is an optimization problem of two variate $\mathcal{D}$ and α_{ijt}, so sparse representation and dictionary update are involved in the solution. In the optimum iterative procedure of image sequences, $\mathcal{D}$ is fixed and corresponding sparse coefficient vector α_{ijt} is optimized. In the dictionary update, the optimized sparse coefficient matrix A is fixed and $\mathcal{D}$ is updated. Repeat this iteration until tensor dictionary $\mathcal{D}$, which corresponds to the processing image sequences, is obtained.

The second step is to define error rate of the sparse representation. Coefficient matrix A is expected to be more sparse under the premise that error rate of the sparse representation is less than a certain threshold value ε, i.e.

$$\min_{\alpha_{ijt},\mathcal{D}} \left\|\alpha_{ijt}\right\|_0 s.t. \left\| \frac{R_{ijt}\mathcal{Y} - \mathcal{D}\alpha_{ijt}}{\sqrt{\mathcal{D}\alpha_{ijt}}} \right\|_2^2 \le \varepsilon \tag{10}$$

The image denoising begins with the adaptive dictionary $\mathcal{D}$ and the sparsity is guaranteed in the above procedure. The optimization problem can finally be described as:

$$\hat{\mathcal{X}}_k = \arg\min_{\alpha_{ijt},\mathcal{X}} \lambda \left\| \frac{\mathcal{Y} - \mathcal{X}}{\sqrt{\mathcal{X}}} \right\|_2^2 + \sum_{ij\in\Omega} \sum_{t=k-f+1}^{k+f-1} \left\| \mathcal{D}\hat{\alpha}_{ijt} - R_{ijt}\mathcal{X} \right\|_2^2 \tag{11}$$

3 Method and Algorithm

3.1 Sparse Representation

Due to the high sampling frequency in temporal dimension in the ultrasound video signal, we choose to collect the image block sequences that consists of the blocks in the same position from each image frame [12]. The data collecting process is shown in Fig. 5.

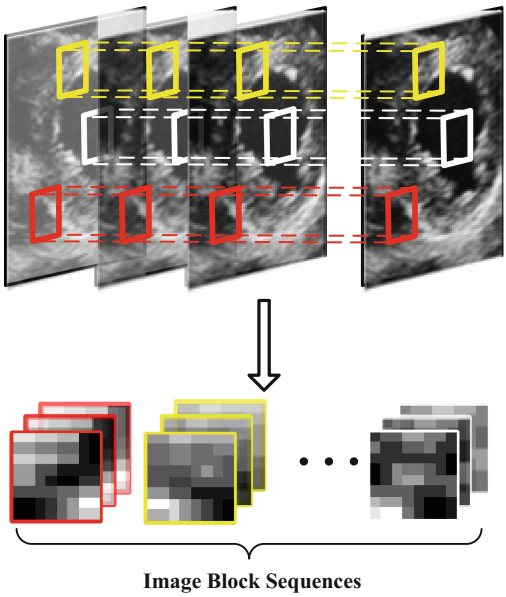

Fig. 5. Image block sequences collecting process

The processed image block sequences contain the information in both spatial dimension and the temporal dimension, and they will be presented sparsely according to the tensor dictionary [13, 14]. To avoid the loss of information of images in either dimension, improved optimization algorithm based on tensor is proposed, called Kruskal Tensor Orthogonal Matching Pursuit (KTOMP).

The steps of KTOMP are summarized in Algorithm 1.

Algorithm 1 Kruskal Tensor Orthogonal Matching Pursuit

1: Input image block sequences with noise $R_{ijt}\mathcal{Y} \in \mathbb{R}^{m\times n\times f}$

2: Initialize projection matrix $D_1 \in \mathbb{R}^{m\times K}$, $D_2 \in \mathbb{R}^{n\times K}$, $D_3 \in \mathbb{R}^{f\times K}$, which are DCT matrices, and $\mathcal{D}_k = \mathcal{1}\times_1 D_1(:,k)\times_2 D_2(:,k)\times_3 D_3(:,k)$ where $\mathcal{1} \in \mathbb{R}^{1\times 1\times 1}$ and $k = 1,2,\ldots,K$.

3: Optimum iterative procedure

Residue $R = R_{ijt}\mathcal{Y}$, $\alpha_{ijt} = \vec{0}$

while $\|\alpha_{ijt}\|_0 \le T_{\max}$ & $\|R\|_F^2 \ge \varepsilon^2$ **do**

Compute the projection $P = R\times_1 D_1'\times_2 D_2'\times_3 D_3'$ where $P \in \mathbb{R}^{K\times K\times K}$

Search $p_{\max}$ in the diagonal of P and the corresponding atom order $k_{\max}$

Replace the residue with $k_{\max}$ th atom $\mathcal{D}_{k_{\max}}$

Compute residual image block

$R = R - (p_{\max}\cdot\mathcal{1})\times_1 D_1(:,k_{\max})\times_2 D_2(:,k_{\max})\times_3 D_3(:,k_{\max})$

Update sparse coefficient vector $\alpha_{ijt}(k_{\max}) = p_{\max}$

end

4: Output sparse coefficient vector α_{ijt} corresponding to $R_{ijt}\mathcal{Y}$

3.2 Initialize Dictionary

In this paper, the dictionary is tensor dictionary and all the elements are rank-one because the data is three-dimensional. Assuming the image blocks and elements are tensors in space $\mathbb{R}^{m\times n\times f}$ and amount of elements is K. To begin with, three DCT matrices are required, i.e. $D_1 \in \mathbb{R}^{m\times K}$, $D_2 \in \mathbb{R}^{n\times K}$, $D_3 \in \mathbb{R}^{f\times K}$. Every atom in the dictionary is generated by normalizing these three matrices and make up a third-order tensor with the same column of each matrix. In this way, we obtain an initial DCT rank-one tensor dictionary, shown in Fig. 6.

3.3 Tensor Dictionary Update

The CANDECOMP/PARAFAC(CP) decomposition [15] is applied to update the tensor dictionary in this method. CP decomposition factorizes a tensor into a sum of

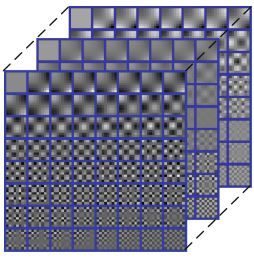

Fig. 6. Initial DCT rank-one tensor dictionary

component rank-one tensors so that atoms in initial dictionary may keep rank-one in the updating process. An error function is defined by:

$$E = \left\| \frac{\mathcal{Y} - \mathcal{D}A}{\sqrt{\mathcal{D}A}} \right\|_F^2 \tag{12}$$

The error function is defined as Frobenius-norm [16] of error tensors. Therefore, we can update the atoms of tensor dictionary by:

$$\begin{aligned} E &= \left\| \frac{\mathcal{Y} - \mathcal{D}A}{\sqrt{\mathcal{D}A}} \right\|_F^2 = \left\| \frac{\mathcal{Y} - \sum_{k=1}^{K} \mathcal{D}_k \alpha_T^k}{\sqrt{\mathcal{D}_k \alpha_T^k}} \right\|_F^2 \\ &= \left\| \frac{\left(\mathcal{Y} - \sum_{k \neq p} \mathcal{D}_k \alpha_T^k \right) - \mathcal{D}_p \alpha_T^p}{\sqrt{\sum_{k=1}^{K} \mathcal{D}_k \alpha_T^k}} \right\|_F^2 = \left\| \frac{E_p - \mathcal{D}_p \alpha_T^p}{\sqrt{\sum_{k=1}^{K} \mathcal{D}_k \alpha_T^k}} \right\|_F^2 \end{aligned} \tag{13}$$

$\mathcal{D}A$ will approach Y after multiple iteration, and the last step is to compute a CP decomposition of E_p in the denominator. In the end, we have optimum $\mathcal{D}_p$ and the corresponding sparse coefficient α_T^p.

3.4 Image Recovery

The optimization problem can be described as (11) and the output is the kth frame $\hat{\mathcal{X}}_k$. Analytic solution is difficult to obtain, so the problem is transformed into a easier one by introducing $\tilde{\lambda}$ as new coefficients. After derivation the solution is expressed as:

$$\hat{\mathcal{X}}_k = \left(\tilde{\lambda} I + \sum_{ij \in \Omega} \sum_{t=k-f+1}^{k} R_{ijt}^T R_{ijt} \right)^{-1} \left(\tilde{\lambda} \mathcal{Y}_k + \sum_{ij \in \Omega} \sum_{t=k-f+1}^{k} R_{ijt}^T D \hat{\alpha}_{ijt} \right) \tag{14}$$

4 Experimental Results

The proportionality coefficient of error rate ε and noise mean variance σ_n is denoted by C. Based on the previous studies, processed cardiac ultrasound images have better PSNR when $C = 8$. The size of image blocks is 8×8, because larger size makes sparse representation a time-consuming process, and smaller size leads to discontinuous blocks between frames. Experiments proved that 3 frames can meet the requirements. The detailed parameters of simulation are summarized in Table 1.

Table 1. Simulation parameters

Methods	Assumptions
Lee	Window size 5 × 5
Kuan	Window size 3 × 3
NCDF	Window size 3 × 3
SRAD	Initial value $Q_0 = 0.5$, $\Delta t = 0.1$
NMWD	Wavelet decomposition level $J = 3$, $\Delta t = 0.1$
SRBF	Window size 3 × 3
CS-based	Image block size 8 × 8, frame $f = 3$, $C = 8$

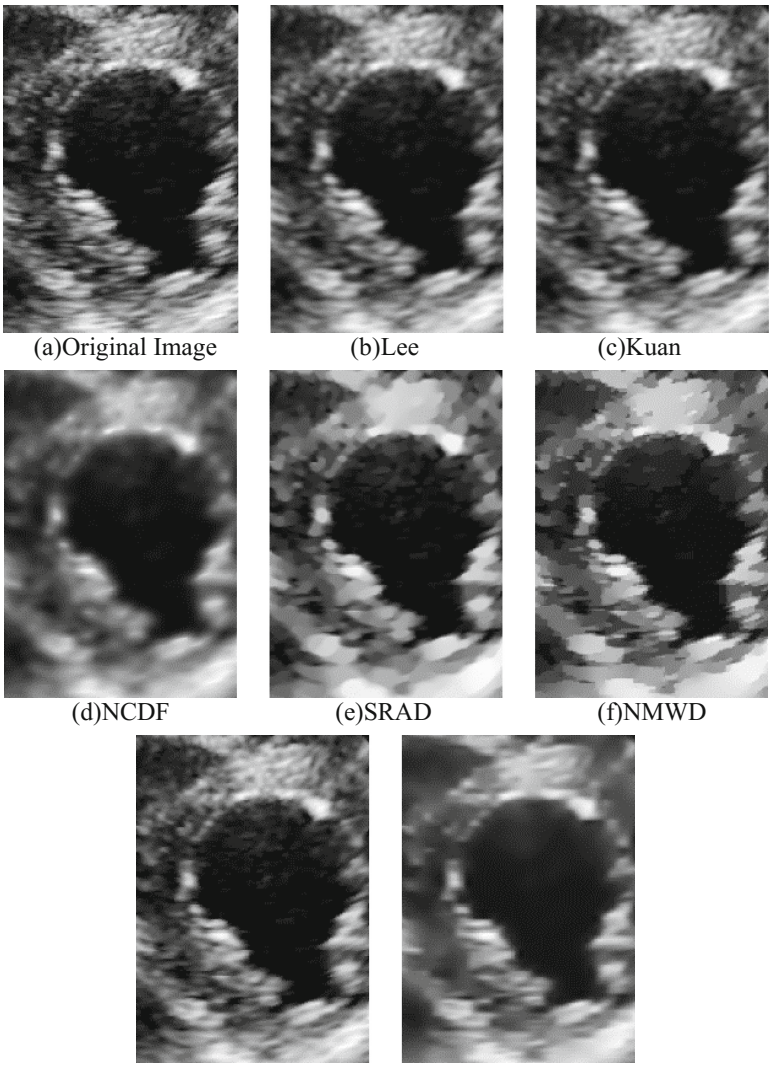

Fig. 7. Denoising performance comparison of CS-based method and traditional methods

Figure 7 demonstrates the CS-based speckle denoising method has better performance in noise reduction and keeps more edge information.

The performance difference is difficult to tell by visual inspection so quantitative results is also required. We compute the remaining noise variance σ_n^2 in the processed images to compare the denoising ability of the methods above. For σ_n^2, lower is better. It is given by:

$$\sigma_n^2 = \frac{\sigma^2}{m} = \frac{\sum_{i=0}^{M-1}\sum_{j=0}^{N-1}[I(i,j) - \bar{I}(i,j)]^2}{\sum_{i=0}^{M-1}\sum_{j=0}^{N-1} I(i,j)} \tag{15}$$

The remaining noise variance of images processed by different methods are summarized in Table 2:

Table 2. Experimental results of σ_n^2

	Experiment 1	Experiment 2	Experiment 3	Experiment 4	Experiment 5
Original	9.2327	6.3542	7.7043	10.6013	9.3056
Lee	3.7621	2.0291	4.1677	5.4885	4.1175
Kuan	5.8392	3.4668	5.3789	7.2655	5.7603
NCDF	2.1080	1.1334	2.9522	3.9787	2.6482
SRAD	7.8007	2.2196	6.3844	8.3852	7.4011
NMWD	1.3690	1.4152	3.9535	6.0422	4.8639
SRBF	8.5283	3.6888	7.3209	9.5148	8.5044
CS-based	**0.3909**	**0.7888**	**2.2784**	**3.1959**	**1.8510**

5 Conclusion

In this paper, we have proposed a CS-based denoising method using tensor model. Considering the temporal redundancy in multi-frame images, video data is divided into image block sequences and represented by tensor models. In addition, an improved OMP based on Kruskal tensor decomposition is utilized in sparse representation. Aiming at the training problem of rank-one tensor dictionary, CP decomposition is applied in the tensor dictionary update. Using the trained dictionary, the noise is separated and the images are recovered in the end. Simulations show that CS-based method outperforms the traditional methods in both visual results and quantitative ones.

Acknowledgement. This work is supported in part by National Natural Science Foundation of China (No. 61671184, No. 61401120, No. 61371100) and National Science and Technology Major Project (No. 2015ZX03001041).

References

1. Lee, J.S.: Digital image enhancement and noise filtering by use of local statistics. IEEE Trans. Pattern Anal. Mach. Intell. **2**, 165–168 (1980)
2. Kuan, D.T., Sawchuk, A.A., Strand, T.C., et al.: Adaptive noise smoothing filter for images with signal-dependent noise. IEEE Trans. Pattern Anal. Mach. Intell. **2**, 165–177 (1985)
3. Perona, P., Malik, J.: Scale-space and edge detection using anisotropic diffusion. IEEE Trans. Pattern Anal. Mach. Intell. **12**(7), 629–639 (1990)
4. Yu, Y., Acton, S.T.: Speckle reducing anisotropic diffusion. IEEE Trans. Image Process. **11** (11), 1260–1270 (2002)
5. Yue, Y., Croitoru, M.M., Bidani, A., et al.: Nonlinear multiscale wavelet diffusion for speckle suppression and edge enhancement in ultrasound images. IEEE Trans. Med. Imaging **25**(3), 297–311 (2006)
6. Salinas, H.M., Fernández, D.C.: Comparison of PDE-based nonlinear diffusion approaches for image enhancement and denoising in optical coherence tomography. IEEE Trans. Med. Imaging **26**(6), 761–771 (2007)
7. Tamara, G., Brett, W.: Tensor decompositions and applications. SIAM Rev. **51**(3), 455–500 (2009)
8. Balocco, S., Gatta, C., Pujol, O., et al.: SRBF: speckle reducing bilateral filtering. Ultrasound Med. Biol. **36**(8), 1353–1363 (2010)
9. Caiafa, C.F., Cichocki, A.: Block sparse representations of tensors using kronecker bases. In: IEEE International Conference on Acoustics, Speech and Signal Processing (ICASSP), pp. 2709–2712. IEEE (2012)
10. Li, X., Shen, H., Zhang, L., Zhang, H., Yuan, Q., Yang, G.: Recovering quantitative remote sensing products contaminated by thick clouds and shadows using multitemporal dictionary learning. IEEE Trans. Geosci. Remote Sens. **52**(11), 7086–7098 (2014)
11. Lu, T., Li, S., Fang, L., Ma, Y., Benediktsson, J.A.: Spectral-spatial adaptive sparse representation for hyperspectral image denoising. IEEE Trans. Geosci. Remote Sens. **54**(1), 373–385 (2016)
12. Selesnick, I.: Total variation denoising via the moreau envelope. IEEE Signal Process. Lett. **24**(2), 216–220 (2017)
13. Lu, Z., Fu, Z., et al.: Learning from weak and noisy labels for semantic segmentation. IEEE Trans. Pattern Anal. Mach. Intell. **39**(3), 486–500 (2017)
14. Cao, Z., Gu, Y.: Sparse representation denoising framework for 3-D building reconstruction from airborne LiDAR data. IEEE J. Sel. Top. Appl. Earth Obs. Remote Sen. **9**(5), 1888–1900 (2016)
15. Rahmani, M., Atia, G.: High dimensional low rank plus sparse matrix decomposition. IEEE Trans. Signal Process. **65**(8), 2004–2019 (2017)
16. Qi, N., Shi, Y., et al.: Multi-dimensional sparse models. IEEE Trans. Pattern Anal. Mach. Intell. **40**(1), 163–178 (2017)